

See discussions, stats, and author profiles for this publication at: <https://www.researchgate.net/publication/263778775>

Role of Single-Walled Carbon Nanotubes on Ester Hydrolysis and Topography of Electrospun Bovine Serum Albumin/Poly(vinyl alcohol) Membranes

ARTICLE in ACS APPLIED MATERIALS & INTERFACES · JULY 2014

Impact Factor: 6.72 · DOI: 10.1021/am502495e · Source: PubMed

CITATION

1

READS

22

4 AUTHORS, INCLUDING:



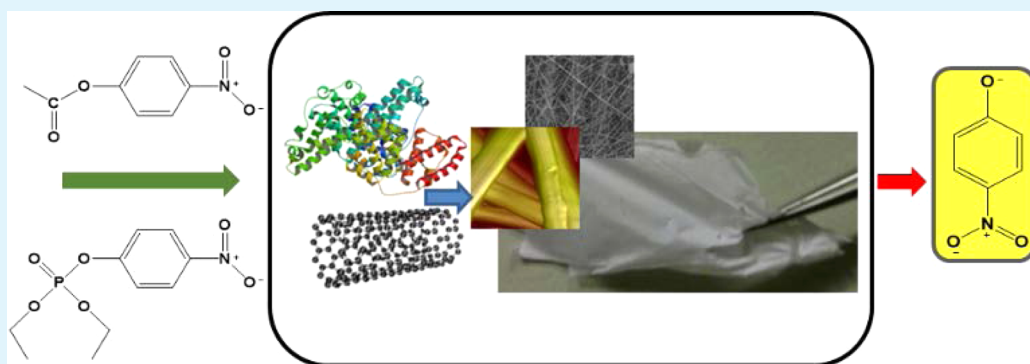
Ramanathan Nagarajan
Pennsylvania State University
113 PUBLICATIONS 4,124 CITATIONS

[SEE PROFILE](#)

Role of Single-Walled Carbon Nanotubes on Ester Hydrolysis and Topography of Electrospun Bovine Serum Albumin/Poly(vinyl alcohol) Membranes

Ericka N. J. Ford, Nisaraporn Suthiwangcharoen, Paola A. D'Angelo, and Ramanathan Nagarajan*

Molecular Sciences and Engineering Team, Natick Soldier Research, Development and Engineering Center, Natick, Massachusetts 01760, United States



ABSTRACT: Electrospun membranes were studied for the chemical deactivation of threat agents by means of enzymatic proteins. Protein loading and the surface chemistry of hybrid nanofibers influenced the efficacy by which embedded enzymes could digest the substrate of interest. Bovine serum albumin (BSA), selected as a model protein, was electrospun into biologically active fibers of poly(vinyl alcohol), PVA. Single-walled carbon nanotubes (SWNTs) were blended within these mixtures to promote protein assembly during the process of electrospinning and subsequently the ester hydrolysis of the substrates. The SWNT incorporation was shown to influence the topography of PVA/BSA nanofibers and enzymatic activity against paraoxon, a simulant for organophosphate agents and a phosphorus analogue of *p*-nitrophenyl acetate (PNA). The esterase activity of BSA against PNA was uncompromised upon its inclusion within nanofibrous membranes because similar amounts of PNA were hydrolyzed by BSA in solution and the electrospun BSA. However, the availability of BSA along the fiber surface was shown to affect the ester hydrolysis of paraoxon. Atomic force microscopy images of nanofibers implicated the surface migration of BSA during the electrospinning of SWNT filled dispersions, especially as greater weight fractions of protein were added to the spinning mixtures. In turn, the PVA/SWNT/BSA nanofibers outperformed the nanotube free PVA/BSA membranes in terms of paraoxon digestion. The results support the development of electrospun polymer nanofiber platforms, modulated by SWNTs for enzyme catalytic applications relevant to soldier protective ensembles.

KEYWORDS: *electrospinning, paraoxon, PVA/BSA/SWNT composite nanofiber, immobilized enzyme activity, nanofiber topography, organophosphates, atomic force microscopy (AFM), ultraviolet visible (UV-vis) spectroscopy, *p*-nitrophenyl acetate (PNA)*

INTRODUCTION

Enzymatic proteins have been identified for diverse applications of industrial and military importance, such as wastewater filtration, cleaning detergents, biofuels, and the molecular decomposition of threat agents.^{1–3} To realize their potential for these applications, it is necessary to immobilize the biologically active enzymes onto the surface of material platforms in order to provide a material framework for the catalytic action of enzyme, to improve enzyme stability, and to allow reuse of the typically expensive enzyme.² The present study of protein immobilized in a polymer nanofiber platform is part of a broader mission to fabricate nonwoven, biofunctionalized nanofiber membranes, for use in Warfighter protective clothing and textiles.

The use of organophosphate compounds, sarin, soman, tabun, and VX as chemical warfare agents (CWAs) and as weapons of terrorism is a serious threat well recognized by all.^{4,5} These compounds are nerve agents because of their inhibition of mammalian acetylcholinesterase activity, an enzyme that plays a critical role in the central nervous system, leading to paralysis and often fatal outcomes. A number of other organophosphate compounds such as paraoxon, para-thion, and malathion are also widely employed as pesticides by the agricultural industry, leading to the toxic contamination of soil and water environments. Because of the high toxicity of

Received: April 24, 2014

Accepted: July 9, 2014

Published: July 9, 2014

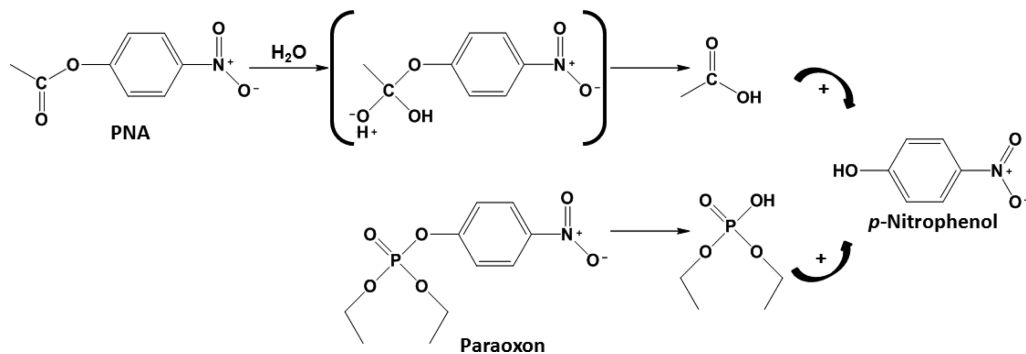


Figure 1. Hydrolysis of *p*-nitrophenol acetate (PNA) and paraoxon.

organophosphate compounds, there is a persisting need for an efficient method to degrade these molecules. The enzyme organophosphate hydrolase (OPH) has shown remarkable activity in the hydrolysis of a broad spectrum of organophosphate neurotoxins.⁶ However, the enzymatic activity of native OPH has been found to be less stable under a variety of storage and operating conditions and this has stimulated active research in synthetic modifications of OPH to overcome these deficiencies. However, the bioengineering methods for the production of OPH and its synthetic modifications are labor intensive and generally associated with low yields,^{7–9} making it essential to engineer a system for the efficient utilization of these enzymes. Given the potential high performance of OPH against organophosphates, its incorporation in a polymer nanofiber platform can be a method to improve its stability and allow reuse of the expensive enzyme.

Prior to working with OPH, we have chosen to work with a readily abundant byproduct of the cattle industry, bovine serum albumin (BSA) esterase, as a model protein, to develop the material platform for functional, nanofibrous membranes that are amendable to threat sensing and chemical deactivation. BSA esterase has shown efficacy toward the decomposition of steroid acetates¹⁰ and *p*-nitrophenyl acetate (PNA).¹¹ Although less efficient than organophosphorus hydrolase (OPH),¹² BSA has also shown reactivity against the paraoxon substrate.¹³ Figure 1 depicts the ester hydrolysis of PNA into *p*-nitrophenol, which under basic conditions, emits a yellow tint that is detectable by use of ultraviolet visible (UV-vis) spectroscopy.¹⁴ The mechanism of base catalyzed PNA hydrolysis is similar to that of analogous organophosphate agents,¹⁵ including ethyl paraoxon (referred to as paraoxon in Figure 1).

The electrospinning technique has been employed to fabricate biologically active membranes in many studies reported in the literature.¹⁶ Applications for bioactive electrospun fibers include filtration, cell growth and regeneration in tissue engineering, biosensing, and chembio protective fabrics.^{17,18} High surface area membranes having fiber diameters on the order of hundreds of nanometers have been prepared by this technique. In a typical electrospinning experiment, the polymer solution is placed in a syringe pump with a needle attached to the end. As the pump displaces the fluid, a droplet of the solution becomes suspended from the needle tip where it is held by surface tension forces. An electrode from a high voltage power supply is placed in contact with the needle tip, applying an electrical potential up to about 30 kV, which induces free charges in the polymer solution. These charged ions move in response to the applied electric field. This introduces a tensile force in the polymer solution.

When the tensile force overcomes the surface tension force associated with the pendent drop of the liquid at the capillary tip, a jet of liquid is ejected from the tip. As the jet travels the short distance of about 10 to 20 cm between the nozzle tip and the collector, the contour length of the jet dramatically increases by many orders of magnitude and the jet thins to nanometer scale. The solvent evaporates as the jet travels from the tip to the collector. The evaporation of the solvent leaves dry nanofibers on the surface of grounded collection plates.¹⁷

Electrospun nanofiber membranes incorporating BSA have been prepared by blending BSA with water swellable polymers: poly(vinyl alcohol), PVA, poly(ethylene oxide), PEO, polycaprolactone, polyurethane, and copolymers.^{19–23} Matrix polymers enable globular BSA, having a molecular weight of 66 kDa, to be electrospun into fibrous mats of up to 50% BSA to the mass of the polymer, a task that cannot be accomplished with solutions solely composed of BSA.²⁰ Active fiber sheaths have been fabricated through the use of coaxial spinning to ensure that the matrix polymer will form the inner core and the protein would be in the outer part of the nanofiber and available to promote substrate digestion.^{21,24} A very interesting alternate approach by Tang et al.¹⁹ is based on electrospinning from a homogeneous solution of BSA and the polymer, but exploits changes in the electric field polarity and differences in molecular polarizability to induce the formation of core–shell nanofibers. The approach takes advantage of the dielectrophoretic force experienced by a molecular species and the resulting molecular transport toward the region of high electric field strength. The time-average dielectrophoretic (DEP) force acting on a spherical particle is given by

$$F_{\text{DEP}} = 2\pi\epsilon_m R^3 \text{CM}(\nabla E^2) \quad (1)$$

where ϵ_m is the absolute permittivity of the surrounding medium, R is the particle radius, CM is the Clausius–Mossotti factor related to the effective polarizability of the particle (which depends on the absolute permittivity of the particle and of the medium), E is the root-mean-square (RMS) amplitude of the electric field, and ∇ is the gradient operator (F and ∇ contribute to the vectorial nature of the equation). Dielectrophoresis leads to the preferential occupation of BSA at the fiber surface with the polarized BSA molecules proceeding toward the surface which is the highest electric field region.^{19,25,26}

Tang et al.¹⁹ clearly demonstrated through multiple methods that BSA migrated toward the surface of PVA nanofibers that were electrospun from tris(hydroxymethyl)aminomethane buffer solution (TBS), having pH values that were either higher or lower than the isoelectric point (pI) of BSA (pI of

4.7). For electrospinning conducted at pH farther from the isoelectric point ($\text{pI} \pm 2$), with either positive or negative applied voltage, analysis using X-ray photoelectron spectroscopy (XPS) showed the presence of nitrogen atoms confirming the presence of BSA in the surface region (defined as the outermost ~ 10 nm thickness where typically the XPS can identify atoms) of the nanofiber. In marked contrast, for electrospinning carried out at $\text{pH} = \text{pI}$, there was no observed nitrogen. In another method, they added colloidal gold to the electrospun nanofibers and conducted scanning electron microscopy (SEM) measurements that could monitor the gold nanoparticles. Because of the well-known strong interactions between the colloidal gold and BSA, one would expect to see the gold nanoparticles near the nanofiber surface if BSA was preferentially located there and the SEM measurements confirmed such a distribution of BSA. They found that gold nanoparticles preferentially adhered to fiber surfaces for nanofibers electrospun from PVA/BSA mixtures at $\text{pH} = \text{pI} \pm 2$.¹⁹ They explained their results in terms of dielectrophoretic motion governed by the charged state of the BSA when pH is away from $\text{pI} \pm 2$, with the dielectrophoretic motion favoring the transport of BSA to the surface. At $\text{pH} = \text{pI}$, both BSA and PVA were uncharged but because PVA has a larger polarizability compared to BSA, a BSA in core surrounded by PVA shell nanofiber was formed. In a different study, core–shell nanofibers of PVA/BSA with PVA dominating the core and BSA preferentially in the shell have been achieved also by increasing the weight percent BSA in proportion to polymer (50:50) and elevating the applied voltage to 22 kV.²⁷

The above-mentioned studies have established that BSA can be moved to the surface region of PVA nanofibers by selecting the pH for electrospinning. Further, the BSA/PVA mass ratio and applied voltage for electrospinning can serve as additional parameters to manipulate the driving of BSA to the nanofiber surface. Because the goal of our study is to achieve catalytically active BSA on the nanofiber, it is preferable to have the protein at the nanofiber–solution interface with direct access to the substrate, instead of in the near surface region that could be as thick as 10 nm. We hypothesized that by including single wall carbon nanotubes (SWNTs) in the nanofiber, which interact nonspecifically with both BSA^{28–30} and PVA,³¹ we may be able to influence the movement of BSA not just to the surface region sampled by the XPS as in the PVA/BSA nanofibers but even closer to the interface to be in direct contact with water. A secondary benefit from the use of SWNTs within the nanofiber is the possibility that we can also develop a SWNT-based analyte sensing method.²⁹ To judge the presence of BSA at the interface with water (if this is promoted by the interactions with the SWNT), we can monitor the esterase activity of electrospun BSA nanofibers. A comparison of the catalytic activity per unit mass of enzyme in the nanofiber platform versus in the aqueous solution will provide a semiquantitative, if not quantitative, measure of the presence of BSA in contact with water. Further, because the interfacial presence of BSA would make the nanofiber more adhesive, the adhesion force at the interface determined by atomic force microscopy will provide another measure of the presence of BSA in contact with water. Therefore, in this study, we have focused on determining the catalytic activity of BSA in the nanofiber platform and the adhesive force at the nanofiber interface as two critical metrics for the development of protein immobilized polymer nanofibers.

MATERIALS AND METHODS

Materials. PVA, having a molecular weight of 100 kDa and 99% hydrolysis (Product No: 341584), and BSA (Product No: A2153-10G) were purchased from Sigma-Aldrich. These were used to prepare electrospinning solutions. Pristine SWNTs (Batch PO342 from Carbon Nanotechnologies Inc., CNI) were used as-received in the formulation of SWNT dispersions. The individual nanotubes present in the CNI sample and their chirality have been identified in our previous unpublished work (for a different batch of the same product) by first debundling and dispersing the nanotubes in water using block copolymer surfactants and applying Raman spectroscopy, fluorescence, and UV-vis spectroscopy to the aqueous dispersions. We were able to identify at least 11 types of metallic nanotubes and 7 types of semiconducting nanotubes in the sample; further, the absence of a broadening G-band in the Raman spectra shows that the bulk of the sample has a semiconducting character. Millipore water and buffer solutions were vacuum filtered through 200 nm pores prior to their use in polymer solutions and protein assays. The following solvents were used to electospin fiber mats and to test the esterase activity of BSA: TBS (at 50 mM and pH 8.1), phosphate buffer (1X) solution (PBS with pH 7.4), and N-2-hydroxyethyl-piperazine-N-2-ethanesulfonic acid (HEPES) buffer (having 50 mM HEPES, 50 mL of sodium chloride, and 0.1 mM magnesium chloride at pH 8.1). Measurements of fluid pH and conductivity were performed using the Accumet AB15 Basic benchtop pH/mV meter (Cole-Parmer) and CDH221 conductivity meter (Omega Engineering Inc.)

Preparation of Electrospin Solutions and Electrospinning. PVA was dissolved in aqueous solutions at temperatures of ~ 85 °C. Concentrated polymer solutions and polymer/SWNT dispersions both were maintained at a clearing temperature of 85 °C until usage, so as to prevent the physical gelation of PVA at room temperature. To prepare unfilled nanofibers (that is, without SWNTs), 22 g/dL PVA was dissolved in TBS or water, used as stock solutions, cooled to room temperature, and diluted with BSA dissolved in water. The concentration of BSA was varied from 0 to 15% of the mass of the PVA in solution. To prepare filled nanofibers, concentrated mixtures of PVA and SWNTs, containing 0.24% SWNTs to the mass of polymer, were prepared from the aqueous dispersion of SWNTs sonicated in the presence of PVA for 24 h at 900 W. Stock PVA/SWNT dispersions in TBS and water were concentrated to 19 and 21 g/dL, respectively. Afterward, stock mixtures were blended with aqueous BSA solutions, so as to prepare hybrid PVA/BSA/SWNT solutions with 0–15% BSA to polymer.

Fiber membranes were electrospun using a positive bias at voltage of 15 kV and polymer feed rates of 0.25–1 mL/h. Aluminum foil collectors were vertically placed 8 cm below the blunt tip syringe needle, having an inner diameter of 0.34 mm (23 gauge).

Determination of Fiber Diameter by SEM. Fiber mats were characterized with scanning electron microscopy (SEM). Membranes adhering to the foil collector were punched out, attached to SEM stubs, and sputter coated with gold/palladium. ImageJ software (US National Institutes of Health) was used to process SEM images from various fiber mats and to determine diameter distributions for at least 50 cross sections.

Determination of Surface Roughness and Adhesion by Atomic Force Microscopy (AFM). Height, root-mean-square (RMS) roughness, and adhesion force profiles were captured using a Dimension Icon AFM equipped with PeakForce QNM (Bruker Corporation). Bruker RFESP silicon tips having a radius of 8 nm, spring constant of 3 N/m, and a resonant frequency of 0.7–1 Hz were used. Calibration of tips was done prior to imaging. The deflection sensitivity was calculated before each experiment using the constant compliance region of force curves taken on bare foil. Cantilever spring constants were calculated using the thermal noise method built in the AFM system. Images were acquired in PeakForce tapping mode in air at 1 Hz and 512 samples/line. Surface roughness was determined from height images where at least 25 areas measuring 200 nm² were analyzed. Adhesion measurements are the result of retraction force curves, which are indications of surface-tip adhesion by means of

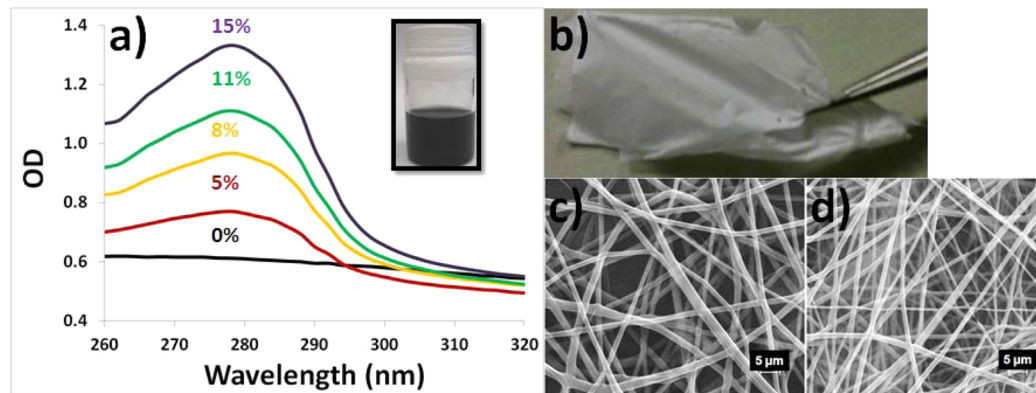


Figure 2. UV-vis spectra of BSA blended within PVA dissolved in water at (a) BSA loadings of 0, 5, 8, 11, and 15% PVA are shown in order from the lowest to highest intensity spectrum. PVA/SWNT fiber mats were obtained after electrospinning. (b) SEM images of PVA/SWNT mats that were electrospun from (c) 0% and (d) 15% BSA mixtures in PVA/water are shown.

Table 1. Diameter of Electrospun PVA and PVA/SWNT Composite Membranes with Increasing Incorporation of BSA^a

BSA (%)	PVA/TBS		PVA/water		PVA/SWNT/TBS		PVA/SWNT/water	
	PVA (wt %) ^b	diameter (nm)	PVA (wt %)	diameter (nm)	PVA (wt %)	diameter (nm)	PVA (wt %)	diameter (nm)
0	17	505 ± 190	12	373 ± 82	16	639 ± 202	15	521 ± 112
5	15	516 ± 210	13	739 ± 135	14	531 ± 165	13	313 ± 75
8	15	610 ± 213	15	709 ± 126	14	408 ± 99	13	310 ± 120
15	15	484 ± 150	15	694 ± 232	14	584 ± 175	13	212 ± 88

^aPercent with respect to the PVA mass. ^bPVA (wt %) refers to the final weight percent of polymer in the electrospinning mixtures.

intermolecular binding or repulsion due to opposing forces. The weight-average of adhesion (nN) was calculated from the force distributions of five fibers; error bars were calculated from the weighted standard deviation.

Protein Assays for Catalytic Activity. Measurements of BSA in the polymer solution as well as the esterase activity of BSA were performed with an EON UV-vis microplate spectrophotometer (BioTek Instruments) and the procedures were adapted from previous studies.^{32,33} Changes in the concentration of BSA within the spinning solutions were measured with the Take-3 accessory by recording the spectra of sample droplets over the wavelength range of 200–800 nm. The ester hydrolysis of PNA and paraoxon in the presence of BSA was assessed by optical density (OD) measurements at 405 nm. The appropriate blanks were subtracted from the raw measurements of OD, so that the reported OD measurements only represented the formation of the hydrolysis product, *p*-nitrophenol. Mixtures of substrate in buffer solution served as the blanks for assays of BSA in solution with the substrate. Control membranes of PVA and PVA/SWNT in the appropriate buffer and substrate served as the blanks for protein assays of BSA embedded within polymer. The OD of the blank was subtracted from the OD of the test specimen; these calculated values were reported herein as the OD of substrate hydrolysis.

Standard BSA solutions were prepared from a stock of 10 mg/mL, which was diluted to concentrations of 0.15–1.65 mg/mL in either PBS at pH 7.4 or HEPES at pH 8.1. These were used in the experiments to determine the catalytic activity of BSA in solution. Electrospun fiber mats were added to buffer to prepare the same nominal concentration of BSA as in the control aqueous protein solutions. Spun fiber mats were assumed to have negligible mass of residual solvent. Membranes of ~5 mg were removed from aluminum collection plates and added to 1 mL of buffer solution. BSA nominal concentrations of 0.25–1.5 mg/mL were prepared from hybrid BSA fiber membranes.

Test protocols for PNA and paraoxon hydrolysis are as follows. PNA substrates, at 11 mM in acetonitrile, were diluted to 0.55 mM in PBS for hydrolysis testing. Samples composed of BSA in aqueous solution or BSA-based fiber membranes; these were incubated at 30 °C and shaken for 1 h in the presence of the substrate. Aliquots of 200

μL were extracted from BSA test samples and dispensed into the openings of 96-well plates for testing. The average OD of four replicates was recorded for each specimen. Assays pertaining to the hydrolysis of paraoxon were performed in HEPES. The paraoxon stock solution was prepared at 2 mM in 10% v/v methanol in HEPES. Paraoxon was diluted to 0.1 mM upon its addition to BSA test samples that were incubated at 30 °C for 48 h while shaking. Calibration curves, derived from 3 mM *p*-nitrophenol in PBS and HEPES, were used to quantify enzymatic degradation.

RESULTS AND DISCUSSION

Enzymatic Activity of BSA Esterase. UV-vis spectroscopy confirmed the presence of BSA within the electrospinning solutions. The spectral intensity of BSA at 278 nm increased in relation to the concentration of BSA within dispersions of PVA/SWNTs in water (Figure 2a). OD peaks became more intense as the BSA concentration increased from 0 to 15%.

Mixtures of PVA/BSA and PVA/SWNT/BSA were electrospun into fiber mats that were later peeled off from the foil surface. Fibers spun from PVA/SWNT/BSA mixtures in TBS did not result in extractable fiber membranes. Its fibers appeared to spray away from each other, which prevented the formation of densely entangled fiber mats. This phenomenon was even more obvious at voltages greater than 15 kV. Tang et al.¹⁹ had concluded that the hydroxyl moieties belonging to PVA will deprotonate under alkaline conditions and carry a negative charge, based on rheological measurements of solution dynamics. They found that the dependence of specific viscosity on polymer concentration below and above the entanglement concentration indicates the PVA solution behaved like a polyelectrolyte. Therefore, having both anionic PVA and anionic BSA may have heightened charge accumulation on the fiber surface to the point of excessive spreading. Water was a better solvent in preparing PVA/BSA/SWNT composite mixtures in that removable membranes were electrospun onto

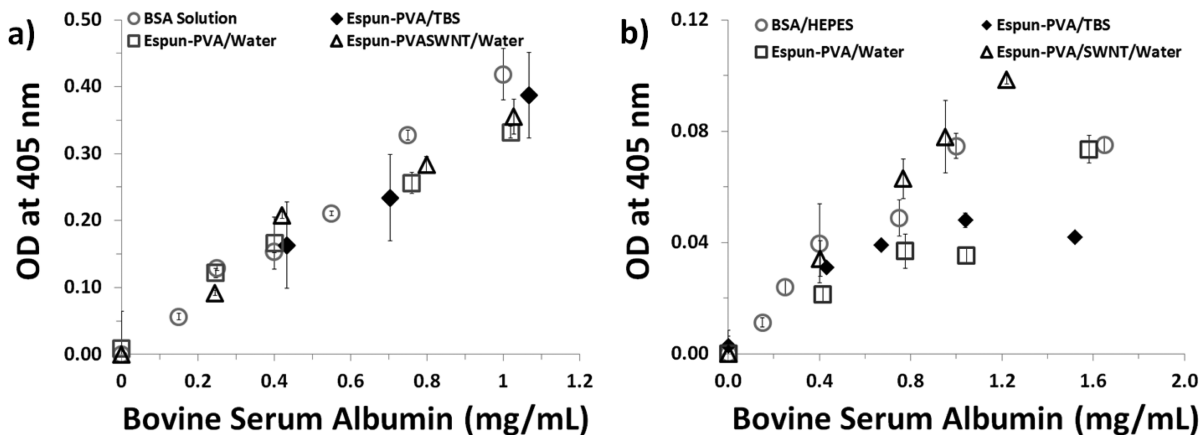


Figure 3. Ester hydrolysis of (a) PNA at 30 °C after 1 h and (b) paraoxon at 30 °C after 48 h, respectively, in the presence of BSA was qualitatively determined from OD measurements at 405 nm. The concentration of BSA was varied for standard test solutions of aqueous BSA (○) and BSA confined to fiber mats electrospun from PVA/TBS (◆), PVA/water (□), and PVA/SWNT/water (Δ).

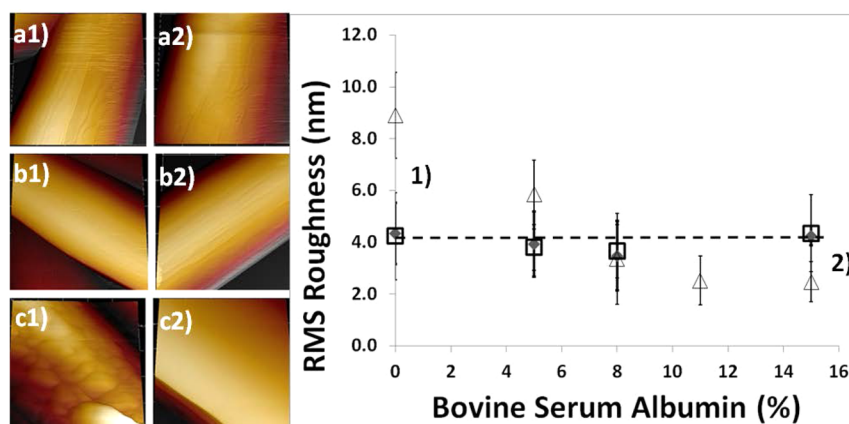


Figure 4. Three-dimensional AFM height profiles of cylindrical fibers that were electrospun from PVA dissolved in (a) water, (b) TBS, and (c) PVA/SWNTs in water are shown. Designations of (1) and (2) represent 0 and 15% BSA, respectively. The concentration of BSA was varied for BSA confined to fiber mats electrospun from PVA/TBS (◆), PVA/water (□), and PVA/SWNT/water (Δ). The root-mean-square (RMS) of depth profiles were used to measure the roughness of fibers having different amounts of BSA.

the collector plate. An example PVA/SWNT fiber mat that was spun from a dispersion prepared in water is shown in Figure 2b–d.

The diameter of electrospun fibers are shown in Table 1. Stock solutions of polymer were diluted with water and aqueous BSA so as to yield fiber mats that could be used in protein assays. Electrospun mixtures yielded fibers averaging less than 1 μm in diameter. The thinnest fibers of \sim 200 nm were obtained from the PVA/SWNT dispersions at 15% BSA.

Protein active nanofiber membranes were tested for catalytic activity in buffer at pH > 7. Nearly half the mass of these uncross-linked membranes could be retrieved after testing. The byproduct of PNA and paraoxon hydrolyzed under basic conditions are represented by the OD measurements shown in Figure 3. Nucleophilic attack of the carbonyl carbon by a hydroxide ion is characteristic of base catalyzed ester hydrolysis and will result in the intermediates and reaction products shown in Figure 1.¹⁴ OD measurements at 405 nm represented the formation of *p*-nitrophenol that took the form of *p*-nitrophenoxide under these basic conditions.

In both cases (PNA or paraoxon as substrates), the presence of *p*-nitrophenol increased with higher concentrations of BSA in solution and electrospun membranes. Figure 3a describes PNA digestion and shows overlapping OD measurements,

which would suggest no difference between the enzymatic activities of BSA in solution versus that of electrospun BSA. Using a calibration curve, 0.06 mM *p*-nitrophenol was digested by 1 mg/mL of BSA in 1 h. Neither matrix of PVA nor PVA/SWNT compromised the activity of BSA toward PNA; thus, the electrospinning technique proves to be an effective means of producing biologically active membranes.

BSA efficacy against paraoxon was significantly lower than the activity against PNA (Figure 3b). At 1 mg/L of BSA in 48 h, only 6.9 μM of *p*-nitrophenol was produced. In contrast to PNA, paraoxon digestion did show some dependency with matrix preparation. The PVA/BSA membranes did not hydrolyze paraoxon as well as the control BSA solutions and the PVA/SWNT/BSA composite membranes. For BSA at 1 mg/mL, the OD of *p*-nitrophenol noticeably deviated from values pertaining to the control and PVA/SWNT/BSA membrane (Figure 3b). Therefore, enzymatic digestion is likely influenced by the accessibility of BSA and the substrate's affinity for matrix polymer. Both scenarios are the likely result of electrospinning, wherein charge or polarizability separated molecules can modify the fiber surface.

Nanofiber Topography–Roughness Profile. The nanofiber topography resulting from SWNT incorporation and BSA loading was investigated by AFM, and the changes in the

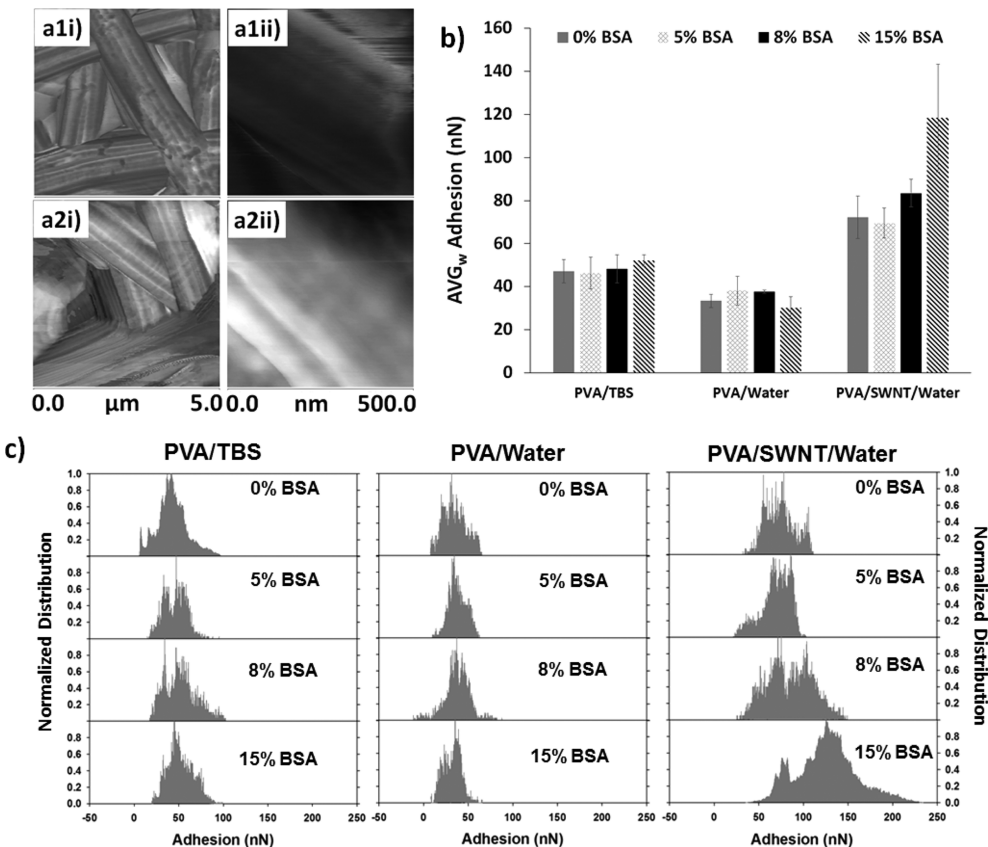


Figure 5. Adhesion profiles were obtained from AFM micrographs of (a1) PVA and (a2) PVA/SWNT fibers at (i) 0% BSA and (ii) 15% BSA. Adhesion forces between the tip–fibers have been quantified for membranes (b) electrospun from PVA dissolved in water, TBS, and water with SWNTs. BSA was added at 0–15% of PVA in solution. The distribution of adhesion forces between the AFM tip and fiber surface are shown for (c) profiles made along the fiber axis.

nanofiber were quantified in terms of surface root-mean-square (RMS) roughness and nonspecific interactions between the silicon AFM tip and fiber surface (Figures 4 and 5, respectively). AFM was chosen as the main technique to study morphology and the mechanical properties of the electrospun fibers, especially since it can provide information about the nanofiber interface most directly.

Three-dimensional height profiles permitted visualization of nanoscale features of the nanofiber. The silicon tip, with a cantilever spring constant of 3 N/m, permitted imaging of nanoscale roughness among control PVA/SWNT fibers, whereas this was not possible with softer AFM tips of spring constant 0.4 N/m when imaging in air. PVA nanofibers were significantly smoother than control PVA/SWNT fibers, whose surface roughness was significantly higher (Figure 4). The PVA/SWNT/BSA composite nanofibers became increasingly less rough as a result of blending higher mass fractions of BSA within PVA/SWNT dispersions. This behavior was noted from height profiles and plots of surface roughness. In contrast, topographies of unfilled PVA/BSA nanofibers were independent of the amount of BSA incorporated and did not vary with higher concentrations of BSA to polymer. Nanoscale roughening among control PVA/SWNT fibers was attributed to SWNT migration toward the fiber surface. The decrease of surface roughness with additional BSA was suggestive of protein migration to the fiber surface. PVA/SWNT/BSA nanofibers at more than 8% BSA were even less rough than unfilled PVA/BSA fibers at similar BSA loading. BSA incorporation reduces polymer viscosity,¹⁹ which would explain

the plasticized flow and smoothness of polymer at the fiber surface. The BSA can also be expected to reduce the solution surface tension that is reflected by the somewhat lower nanofiber diameters in the presence of BSA.

Nanofiber Topography–Adhesion Mapping. Adhesion profiles of electrospun fibers were used to confirm whether or not proteins had migrated to the fiber interface that would be in contact with water. AFM adhesion force (F_{ad} in eq 2) is the sum of all forces between the tip and sample surface; such as electrostatic (F_{el}), capillary forces (F_{cap}), van der Waals (F_{vdW}), and chemical forces (F_{chem}) resulting from hydrogen bonding or charge transfer interactions.³⁴

$$F_{ad} = F_{el} + F_{cap} + F_{vdW} + F_{chem} \quad (2)$$

Intermolecular forces between the tip and the nanofiber surface are represented by tip retraction forces. Because the force measurements are made in air, chemical and van der Waals forces are expected to drive the interactions. Attractive forces between the silicon tip and BSA surface are expected to exceed those from tip-polymer interactions because BSA possesses an abundance of amino acid residues that are conducive to nonspecific binding to the tip.

The most significant result from the AFM adhesion mapping is the difference between the PVA/SWNT nanofibers and the PVA nanofibers when BSA is incorporated into the nanofibers. BSA incorporation did not influence the adhesion profiles of PVA nanofibers that were prepared from mixtures in TBS or water. The magnitude of the adhesion forces between the AFM tip and surface of PVA nanofibers for 0–15% BSA consistently

ranged between 0 to 50 nN. However, significantly higher values of adhesion were observed for PVA/SWNT nanofibers as larger percentages of BSA were incorporated (Figure 5). The distribution of adhesion forces shifted to higher average values (72 to 118 nN) as the percentage of BSA within PVA/SWNT nanofibers increased. These results suggest that the BSA protein is more prone to migration to the interface when fibers were electrospun from SWNT dispersions. Thus, adhesion profiles provided further evidence that “sticky” BSA has migrated to the interface of electrospun fibers. Homogeneous features were observed along the surface of PVA/SWNT/BSA fibers even at 15% BSA (Figure 5a), which confirms good blending between the protein and the matrix polymer. These AFM results support the idea that in the PVA/SWNT nanofibers, core–shell morphologies are obtained with BSA preferentially at the interface. In contrast, in the PVA nanofibers, BSA was not significantly present at the interface. We note that for the latter case, the XPS measurements in ref 19 convincingly showed that the BSA is in the surface region. Therefore, the AFM results suggest that there is a fundamental distinction between the nature of the surface region probed by XPS and that probed by AFM adhesion mapping.

A secondary observation is that the adhesion values for control PVA/SWNT nanofibers were higher than those for the control PVA nanofibers (prepared from PVA dissolved in either water or TBS). This would suggest that the presence of SWNTs instigated a change in the surface chemistry of electrospun PVA. In earlier discussion, we suggested that the nanoscale roughness observed for the control PVA/SWNT nanofibers (Figure 4c1) is due to SWNT migration toward the fiber surface. We propose that the interactions of this migrated SWNT with PVA leads to the concurrent alignment of PVA hydroxyl groups toward the air surface. The proliferation of surface hydroxyl groups would increase the adhesion force contribution that is due to hydrogen bonding between the fiber surface and silicon tip. The migration of SWNT to the surface can result from the DEP effect. In a study of DEP separation, metallic multiwalled carbon nanotubes (MWNTs) were separated from polystyrene microspheres, with the MWNTs concentrated at points of high electric field in contrast to the polymer microspheres, which resided in regimes of low electric field.³⁵ The SWNTs used in the present study include both metallic and semiconducting SWNTs, and the SWNTs are also susceptible to DEP controlled transport. The observed gradual increase in fiber adhesion with 0 to 8% BSA suggest that PVA hydroxyl groups continued to align toward the interface of electrospun composite fibers in the presence of BSA. The overall adhesion force is therefore the sum of nonspecific protein binding and hydrogen bonding with PVA hydroxyl groups as noted by shifts in adhesion force profiles and increases in average adhesion (Figure 5b,c).

Another secondary observation is the difference between the average adhesion forces of PVA nanofibers depending on whether the buffer or water was used. Adhesion force values less than 40 nN were found for fibers electrospun from mixtures in water, whereas values greater than 40 nN were found for fibers electrospun from mixtures in TBS (Figure 5b). Under the positive bias, hydroxyl groups of negatively charged PVA in TBS are expected to align toward the fiber interface, which would account for the differences observed between the adhesion values reported for PVA fibers electrospun from TBS and water mixtures.

CONCLUSION

BSA incorporated within electrospun polymer nanofibers as the material platform was shown to exhibit esterase activity against PNA and paraoxon substrates. The PVA/BSA nanofibers hydrolyzed PNA to the same extent as the BSA in aqueous solution. The BSA activity was not compromised because of its incorporation within the nanofiber. In contrast to this PNA hydrolysis behavior, the nanofiber membranes of PVA/BSA did not hydrolyze paraoxon to the same extent as the BSA in solution. Interestingly, paraoxon expressed less affinity for the solvated PVA membranes than PNA and the substrate's affinity for matrix polymer appeared to influence its ability to access the enzymatic protein. While PNA readily diffused through the nanofiber mat of the solvent swollen PVA membrane, similar access for paraoxon was likely restricted by the ethyl phosphate moiety. Paraoxon accessibility to the nanofiber membrane was greatly improved in the PVA/SWNT/BSA nanofibers where the protein had assembled toward the fiber interface. The inclusion of the SWNTs within biohybrid membranes of PVA/BSA promoted the assembly of BSA along the interface of nanofibers, as confirmed by AFM roughness and adhesion profiles of electrospun fibers. This approach of blending protein, SWNTs, and water-soluble polymer offers a simple method to electrospinning biologically active core–shell fibers without the use of coaxial extrusion or dip coating. Most importantly, active proteins remained accessible to the substrate regardless of its affinity with the host polymer. This study confirms that the polymer nanofiber platform modulated by SWNTs can be a viable approach to the engineering exploitation of enzyme catalytic applications.

AUTHOR INFORMATION

Corresponding Author

*R. Nagarajan. Address: Molecular Sciences and Engineering Team Natick Soldier Research, Development, and Engineering Center, 15 Kansas Street, Natick, MA 01760. Phone: 508 233 6445. Fax: 508 233 4469. E-mail: Ramanathan.nagarajan.civ@mail.mil.

Notes

The authors declare no competing financial interest.

ACKNOWLEDGMENTS

This research was funded by the National Research Council of the National Academies Research Associateship award to conduct research in the area of Chemical and Biological Defense Science and Technology. In addition, this research was supported in part by an appointment to the Postgraduate Research Participation Program at the US Army Natick Soldier Research, Development and Engineering Center (NSRDEC) administered by the Oak Ridge Institute for Science and Education through an interagency agreement between the US Department of Energy and NSRDEC. The authors also thank Chuck Hewitt and Kevin Narang for measuring the fiber diameters obtained from SEM micrographs.

REFERENCES

- (1) Khan, A. A.; Alzohairy, M. A. Recent Advances and Applications of Immobilized Enzyme Technologies: A Review. *Res. J. Biol. Sci.* **2010**, *5*, S65–S75.
- (2) Nisha, S.; Karthick, S. A.; Gobi, N. A Review on Methods, Application and Properties of Immobilized Enzyme. *Chem. Sci. Rev. Lett.* **2012**, *1*, 148–155.

- (3) Russell, A. J.; Berberich, J. A.; Drevon, G. F.; Koepsel, R. R. Biomaterials for Mediation of Chemical and Biological Warfare Agents. *Annu. Rev. Biomed. Eng.* **2003**, *5*, 1–27.
- (4) Benning, M. M.; Kuo, J. M.; Raushel, F. M.; Holden, H. M. Three-Dimensional Structure of Phosphotriesterase: An Enzyme Capable of Detoxifying Organophosphate Nerve Agents. *Biochemistry* **1994**, *33*, 15001–7.
- (5) Huo, D.; Yang, L.; Hou, C.; Fa, H.; Luo, X.; Lu, Y.; Zheng, X.; Yang, J. Molecular Interactions of Monosulfonate Tetraphenylporphyrin (TPPS1) and Meso-tetra(4-sulfonatophenyl)porphyrin (TPPS) with Dimethyl Methylphosphonate (DMMP). *Spectrochim. Acta, Part A* **2009**, *74*, 336–43.
- (6) Efremenko, E. N.; Sergeeva, V. S. Organophosphate Hydrolase - An Enzyme Catalyzing Degradation of Phosphorus-Containing Toxins and Pesticides. *Russ. Chem. Bull.* **2001**, *50*, 1826.
- (7) Votchitseva, Y. A.; Efremenko, E. N.; Aliev, T. K.; Varfolomeyev, S. D. Properties of Hexahistidine-Tagged Organophosphate Hydrolase. *Biochemistry* **2006**, *71*, 167–72.
- (8) Kim, M.; Gkikas, M.; Huang, A.; Kang, J. W.; Suthiwangcharoen, N.; Nagarajan, R.; Olsen, B. D. Enhanced Activity and Stability of Organophosphorus Hydrolase via Interaction with an Amphiphilic Polymer. *Chem. Commun. (Cambridge, U. K.)* **2014**, *50*, 5345–8.
- (9) Suthiwangcharoen, N.; Nagarajan, R. Enhancing Enzyme Stability by Construction of Polymer–Enzyme Conjugate Micelles for Decontamination of Organophosphate Agents. *Biomacromolecules* **2014**, *15*, 1142–1152.
- (10) Rongone, E. L.; Bocklage, B. C.; Strength, D. R.; Doisy, E. A. Hydrolysis of Steroid Acetates by Bovine Albumin. *J. Biol. Chem.* **1957**, *225*, 969–975.
- (11) Awad-Elkarim, A.; Means, G. E. The Reactivity of p-Nitrophenyl Acetate with Serum Albumins. *Comp. Biochem. Physiol., Part B: Biochem. Mol. Biol.* **1988**, *91*, 267–272.
- (12) Singh, A.; Lee, Y.; Dressick, W. J. Self-Cleaning Fabrics for Decontamination of Organophosphorous Pesticides and Related Chemical Agents. *Adv. Mater.* **2004**, *16*, 2112–2115.
- (13) Sultatos, L. G.; Basker, K. M.; Shao, M.; Murphy, S. D. The Interaction of the Phosphorothioate Insecticides Chlorpyrifos and Parathion and Their Oxygen Analogues with Bovine Serum Albumin. *Mol. Pharmacol.* **1983**, *26*, 99–104.
- (14) Goren, J. H.; Fridkin, M. The Hydrolysis of p-Nitrophenylacetate in Water. *Eur. J. Biochem.* **1974**, *41*, 263–272.
- (15) Kawanami, Y.; Yunoki, T.; Nakamura, A.; Fujii, K.; Umano, K.; Yamauchi, H.; Masuda, K. Imprinted Polymer Catalysts for the Hydrolysis of p-Nitrophenyl Acetate. *J. Mol. Catal. A: Chem.* **1999**, *145*, 107–110.
- (16) Agarwal, S.; Wendorff, J. H.; Greiner, A. Use of Electrospinning Technique for Biomedical Applications. *Polymer* **2008**, *49*, 5603–5621.
- (17) Reneker, D. H.; Yarin, A. L.; Zussman, E.; Xu, H. Electrospinning of Nanofibers from Polymer Solutions and Melts. *Adv. Appl. Mech.* **2007**, *41*, 44–195.
- (18) Picciani, P. H. S.; Medeiros, E. S.; Orts, W. J. O.; Mattoso, L. H. C. Advances in Electroactive Electrospun Nanofibers. In *Nanofibers - Production, Properties and Functional Applications*; Lin, T., Ed.; InTech: Rijeka, Croatia, 2011; p 116.
- (19) Tang, C.; Ozcam, A. E.; Stout, B.; Khan, S. A. Effect of pH on Protein Distribution in Electrospun PVA/BSA Composite Nanofibers. *Biomacromolecules* **2012**, *13*, 1269–1278.
- (20) Kowalczyk, T.; Nowicka, A.; Elbaum, D.; Kowalewski, T. A. Electrospinning of Bovine Serum Albumin. Optimization and the Use for Production of Biosensors. *Biomacromolecules* **2008**, *9*, 2087–2090.
- (21) Su, Y.; Mo, X. Dual Drug Release from Coaxial Electrospun Nanofibers. *J. Controlled Release* **2011**, *152*, e82–e84.
- (22) Sanders, E. H.; Kloefkorn, R.; Bowlin, G. L.; Simpson, D. G.; Badr, R.; Wnek, G. E. Microencapsulation of Aqueous Domains within Electrospun Polymer Fibers. *Polym. Prepr. (Am. Chem. Soc., Div. Polym. Chem.)* **2003**, *44*, 78.
- (23) Bernfeld, P.; Wan, J. Antigens and Enzymes Made Insoluble by Entrapping them into the Lattices of Synthetic Polymers. *Science* **1963**, *142*, 678–679.
- (24) Yarin, A. L.; Zussman, E.; Wendorff, J. H.; Greiner, A. Material Encapsulation and Transport in Core-Shell Micro/Nanofibers, Polymer and Carbon Nanotubes and Micro/Nanochannels. *J. Mater. Chem.* **2007**, *17*, 2582–2599.
- (25) Stachewicz, U.; Stone, C. A.; Willis, C. R.; Barber, A. H. Charge Assisted Tailoring of Chemical Functionality at Electrospun Nanofiber Surfaces. *J. Mater. Chem.* **2012**, *22*, 22935–22941.
- (26) Lancuski, A.; Fort, S.; Bossard, F. Electrospun Azido-PCL Nanofibers for Enhanced Surface Functionalization by Click Chemistry. *ACS Appl. Mater. Interfaces* **2012**, *4*, 6499–6504.
- (27) Won, J. J.; Nirmala, R.; Navamathanavan, R.; Kim, H. Y. Electrospun Core-Shell Nanofibers From Homogeneous Solution of Poly(Vinyl Alcohol)/Bovine Serum Albumin. *Int. J. Biol. Macromol.* **2012**, *50*, 1292–1298.
- (28) Li, L.; Lin, R.; He, H.; Sun, M.; Jiang, L.; Gao, M. Interaction of amidated single-walled carbon nanotubes with protein by multiple spectroscopic methods. *J. Lumin.* **2014**, *145*, 125–131.
- (29) Yang, W.; Ratinac, K. R.; Ringer, S. P.; Thordarson, P.; Gooding, J. J.; Braet, F. Carbon Nanomaterials in Biosensors: Should You Use Nanotubes or Graphene? *Angew. Chem., Int. Ed.* **2010**, *49*, 2114–2138.
- (30) Du, J.; Ge, C.; Liu, Y.; Bai, R.; Li, D.; Yang, Y.; Liao, L.; Chen, C. The Interaction of Serum Proteins with Carbon Nanotubes Depend on the Physicochemical Properties of Nanotubes. *J. Nanosci. Nanotechnol.* **2011**, *11*, 10102–10110.
- (31) Ford, E. N. J.; Minus, M. L.; Liu, T.; Choi, J. I.; Jang, S. S. J.; Kumar, S. Influence of SWNTs on the Preferential Alignment of Molecular Moieties in PVA Fibers. *Macromol. Chem. Phys.* **2012**, *213*, 617–626.
- (32) De, P.; Li, M.; Gondi, S. R.; Sumerlin, B. S. Temperature-Regulated Activity of Responsive Polymer-Protein Conjugates Prepared by Grafting-from via RAFT Polymerization. *J. Am. Chem. Soc.* **2008**, *130*, 11288–9.
- (33) Suthiwangcharoen, N.; Li, T.; Wu, L.; Reno, H. B.; Thompson, P.; Wang, Q. Facile Co-Assembly Process to Generate Core-Shell Nanoparticles with Functional Protein Corona. *Biomacromolecules* **2014**, *15*, 948–56.
- (34) Butt, H.-J.; Cappella, B.; Kappi, M. Force Measurements with the Atomic Force Microscope: Technique, Interpretation and Applications. *Surf. Sci. Rep.* **2005**, *59*, 1–152.
- (35) Zhang, C.; Khoshmanesh, K.; Tovar-Lopez, F. J.; Mitchell, A.; Włodarski, W.; Klantar-zadeh, K. Dielectrophoretic Separation of Carbon Nanotubes and Polystyrene Microparticles. *Microfluid. Nanofluid.* **2009**, *7*, 633–645.
- (36) Jung, D.; Minami, I.; Patel, S.; Lee, J.; Jiang, B.; Yuan, Q.; Li, L. K.; Sachiko; Chen, Y.; Lee, K.-B.; Nakatsuji, N. Incorporation of Functionalized Gold Nanoparticles into Nanofibers for Enhanced Attachment and Differentiation of Mammalian Cells. *J. Nanobiotechnol.* **2012**, *10*, 1–10.